ARTICLE

In silico optimization of the Benzofuropyridine core structure as CDK-5 inhibitor

Reymark C. Ereje

Department of Physical Sciences, College of Science, University of the Philippines Baguio, Baguio City, Benguet, Philippines 2600

ABSTRACT

Cyclin-dependent kinase-5 (CDK-5) is a phosphorylating enzyme known for its function in neuronal disorders. Benzofuropyridines (BFP) are a class of heteroaromatic molecules that inhibit CDK-5. Known structural derivatives of this compound remain scarce, prompting the use of computational methods to produce more potent derivatives. In this study, three derivatization strategies were employed to design the **BX-1-1** (45 analogs), **B1-X-1** (33 analogs), and **B1-1-X** (26 analogs) series. These analogs were evaluated using computational tools such as molecular docking, SwissADME and molecular dynamics simulations. Results showed that the **BX-1-1** series, focusing on the functionalization of the 2-O position of BFP, showed the greatest potential for structural diversification as inhibitors, with the **B29-1-1** analog having the highest binding energy of -10.7 kcal/mol. Key residues, such as *Phe80*, *Cys83*, and *Lys33*, with their specific interactions with the 9 BFP representative analogs were identified. The drug-like properties of the compounds were assessed, and the results demonstrated the potential of the analogs for drug development, with good bioavailability scores and optimum synthetic accessibility. Moreover, **B1-11-1** and **B1-1-18** (binding energies: -9.5 and -10.2 kcal/mol respectively) are two lead compounds having high affinity for CDK-5 and good potential to permeate the Blood-Brain Barrier. The CDK-5 enzyme alone remained stable, but the **B29-1-1** ligand-protein complex exhibited limited stability over the 100-nanosecond molecular dynamics simulation. Overall, this work provided valuable insights into the future design of BFP as CDK-5 inhibitors using computational tools.

INTRODUCTION

Cyclin-dependent kinases (CDKs) are members of the serine-threonine kinase family that are primarily involved in neuronal degradation and cell cycle regulation, making them prominent targets for drug discovery (Asghar et al. 2015; Casimiro et al. 2013). Cyclin-dependent kinase-5 (CDK-5), a member of the mentioned kinase group, is an enzyme normally found in post-mitotic neurons generally involved in brain development (Dhavan and Tsai 2001). The native and physiological form of CDK-5 consists of a 32 kilodalton (kDa) catalytic unit that is normally attached to a 33-36 kDa subunit, known as p35, that serves as an activator of the enzyme function. However, overactivation of CDK-5 by p25, the truncated version of p35, causes enzyme dysregulation and is attributed to neurodegeneration such as Alzheimer's disease (Kusakawa et al. 2000). To date, a few compounds such as roscovitine (Asghar et al. 2015) and dinaciclib (Peyressatre et al. 2015) are known to inhibit CDK-5, but *in vivo* trials are still limited.

Benzofuropyridine (BFP) is a tricyclic heterocompound derived from the azacarbazole core structure. The first reported literature on the potential bioactivity of BFP against CDKs was published by Brachwitz et al. (Brachwitz and Hilgeroth 2002; Brachwitz et al. 2003) through functionalizing the C4 position with a phenyl group. In another study by Tell and colleagues in 2012, the group focused on derivatizing the C7 and C8 positions of BFP, revealing improved affinity with CDK-1 and CDK-5, with a 2.1 μM inhibition constant (K_i) against CDK-5 (Tell et al. 2012). One of the more recent developments in the derivatization of the BFP was reported by Holzer and co-workers in 2018 (Holzer et al. 2018), which showed a nanomolar range of activity against CDK-5 enzyme by attaching hydroxy groups at the C3 and C6 positions followed by annelating another benzene ring at the C7 and C8 sites. The structure of BFP, together with its known analogs exhibiting activity against CDK-5, is presented in Figure 1.

To further understand the derivatization pattern and to enhance the bioactivity of small molecules such as the BFP, computational tools are utilized. Computer-aided drug design or CAAD is a technique that uses computer algorithms to analyze drug candidates and molecules with similar biochemical properties (Surabhi and Singh 2018). One commonly used computational tool is molecular docking, which is useful in streamlining the search of potential ligands especially when the crystal structure of the protein target is

*Corresponding author
Email Address: **rcereje@up.edu.ph**
Date received: 18 February 2026
Dates revised: 29 April 2026 and 13 June 2026
Date accepted: 22 June 2026
DOI: https://doi.org/10.54645/2026191KCB-64

KEYWORDS

Benzofuropyridine, CDK-5 enzyme, Molecular docking, Structure-activity Relationship, SwissADME, Optimization, Molecular Dynamics

available. This method involves the interaction of the receptor (usually rigid) with its specified arrays of ligands designed to be docked to the receptor binding site. The binding affinity score of the ligands can later be generated, and the interactions to the protein target can be clearly visualized (Meng et al. 2011).

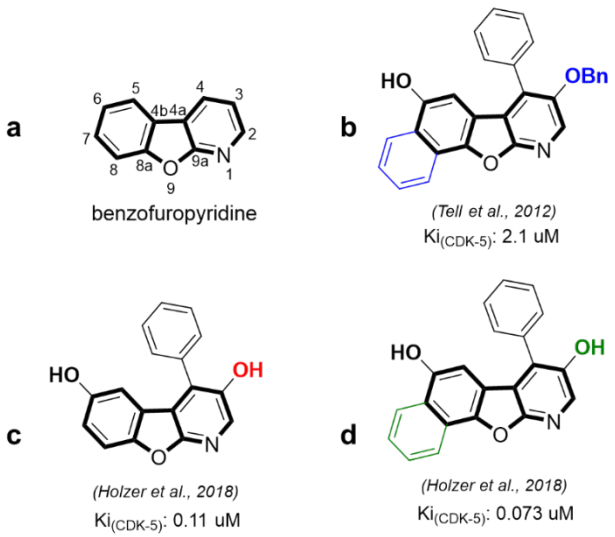

Figure 1: (a) Core structure of benzofuropyridine (BFP). **(b-d)** Known BFP analogs with CDK-5 inhibition activity presented as Ki; **c** as the reference/baseline (ref) compound in this study.

Not only is the interaction of the candidate molecule with its specific target important, but also the concentration and bioavailability of drugs. The Absorption, Distribution, Metabolism and Excretion (ADME) of potential therapeutics also plays a crucial role in drug efficacy (Hay et al. 2014). *In silico* methods in predicting ADME with pharmacokinetic properties are now becoming popular especially in the quest for developing more potent and efficient drug candidates (Tian et al. 2015). Another powerful tool utilized in computational studies is molecular dynamics (MD) simulation. This technique evaluates the stability of the protein and the ligand, examining ligand-induced conformational changes in the protein structure over time (Dong et al. 2016). In this work, computational tools are utilized to optimize the derivatization of the benzofuropyridine core structure, to understand its substitution patterns, and to provide analogs with potential increased inhibition against the target CDK-5 enzyme. Free *in silico* software, such as SwissADME (Daina et al. 2017) was employed to predict drug-like properties of the BFP analogs. A molecular dynamics simulation was performed to investigate the stability of the candidate compound with the enzyme.

MATERIALS AND METHODS

Derivatization Plan

To facilitate the optimization of the core BFP structure, a series of substituent groups was carefully chosen to serve as illustrative analogs. The functionalization strategy for the compound library was driven by integrating three complementary approaches: 1) established synthetic protocols from reported literature on benzofuropyridine (BFP) derivatization, 2) the systematic decision-making framework of the Topliss Tree (Topliss 1972) for optimizing aromatic/aliphatic substituents, and 3) structural insights gained from an initial preparatory docking simulation of the unsubstituted BFP scaffold. A total of 104 BFP compounds were prepared, coming from three distinct series of substitution plans namely: **B**X-1-1 (45 analogs), **B**1-X-1 (33 analogs), and **B**1-1-X (26 analogs). The structures were drawn using the ChemDraw program and the 3-dimensional scaffold was optimized using HyperChem. The substituent positions in the BFP core moiety for each series are presented in Figure 2.

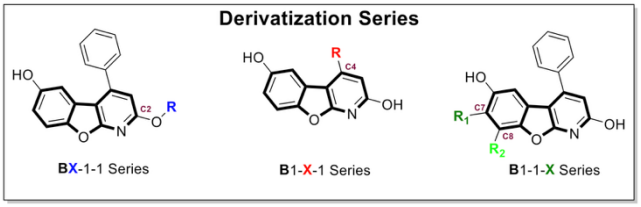

Figure 2: The derivatization plan for the optimization of the BFP core structure. The coding nomenclature is as follows: **B** stands for Benzofuropyridine; and **X** represents the analog number in that series.

Molecular Docking

The crystal structure of the CDK-5 with the truncated p25 (PDB Code: 1UNL) sequence and a co-crystallized roscovitine (RSC) molecule (a known CDK-5 inhibitor) was obtained from the Protein Data Bank (http://www.rcsb.org/PDB). The CDK-5/p25 form was chosen as this is the known pathological isoform of the kinase. Unnecessary molecules such as the co-crystallized ligand, water, and other ions were removed. Hydrogens were added to the enzyme using BIOVIA Discovery Studio program. After which, Kollman charges were added, correct atom assignment was done using AutoDock Tools 1.5.7 (Goodsell and Olson 1990), and the protein structure was saved as .pdbqt format.

The three-dimensional (3D) structures of the 104 identified BFP compounds were drawn, then geometrical optimization was performed using the Semi-empirical AM1 mode (RMS=0.01) in the HyperChem program, and the structure was saved as .mol file. The ligands were further processed by adding Gasteiger charges, identifying rotatable bonds, combining non-polar hydrogens using AutoDock Tools and were finally saved as .pdbqt files.

The center of mass with the x, y, z coordinates (56.89, 28.55, 28.05) served as the binding pocket of the CDK-5 enzyme was determined using the Vega ZZ software. The grid box was set to 30x30x30 cubic angstrom ($Å^3$) dimensions, large enough to directly accommodate BFP ligands, which measure approximately 10x7 $Å^2$ in length and width. Docking of the ligands to the specified binding pocket was done using AutoDock Vina 1.1.2 (Eberhardt et al. 2021) program. The 2D interactions of the BFP analogs to the CDK-5 enzyme were visualized through BIOVIA Discovery Studio Visualizer, and the top-rank binding energy (in kcal/mol) for each ligand was tabulated.

Drug-likeness Prediction

A total of 9 BFP compounds (3 from each series) were analyzed for their potential in drug development using the SwissADME freeware (Daina et al. 2017). Physicochemical and pharmacokinetic parameters were computed, the ADME properties were predicted, and their drug-likeness was assessed using the Lipinski Rule of Five (Lipinski 2004), a known predictor in medicinal chemistry.

Molecular Dynamics Simulation

The structure of the native CDK-5 enzyme was obtained from Protein Data Bank (PDB ID: 1UNL). The downloaded structure was cleaned and modeled using the AMBER99sb-ILDN force field, while the docked ligand coordinates were optimized and parameterized under the General AMBER Force Field (GAFF) framework via topology conversion using ACPYPE. The complex structure was solvated using TIP3P water conditions in a cubic box type. Energy minimization was done under standard NVT and NPT protocols at 300 Kelvin temperature with 1 atm pressure setting. The actual MD simulation was done using GROMACS (Berendsen et al. 1995) software with 100 nanosecond (ns) simulation time at 2 fs time step. All file formats were preserved natively within the workflow without employing external conversion tools. The results were then post-processed to remove periodic boundary conditions, and the Root Mean Square Deviation (RMSD) and Root Mean Square Fluctuation (RMSF) were determined.

RESULTS AND DISCUSSION

Derivatization Strategy

To fully understand the substitution trends and patterns in the optimization of the core BFP structure, numerous substituents needed to be examined to determine the potential Structure-Activity Relationship (SAR) of the BFP derivatives. The main consideration for the creation of derivatives and what substituents are to be appended in the core BFP structure are based on three parameters namely: 1) the available literature on the functionalization of BFP to know which carbon position has the potential to be explored, 2) the Topliss tree parameter for drug design, and 3) pre-docking of the unsubstituted BFP derivative, 2,6-dihydroxybenzofuropyridine (2,6-dHBFP). Reported literature on the actual synthesized benzofuropyridine compounds with tested inhibitory activity against CDK-5 revealed that the C3, C4, C6, C7 and C8 positions of the core moiety are important for improving binding affinity through strong interactions with the target enzyme. In the pioneering work of Brachwitz et al. (Brachwitz and Hilgeroth 2002), the attachment of the 4-phenyl group was a significant substituent for sustained activity while Holzer et al. highlighted the importance of the 3- and 6-OH in improving the K_i value against CDK-5. Consequently, the synthesized BFP with 4-phenyl, 3- and 6-OH substituents (*Figure **1c***) was selected to be the standard or baseline compound (referred to as **ref**) with a binding energy of -9.6 kcal/mol against CDK-5 (Holzer et al. 2018), serving as the basis for affinity improvement by other BFP analogs in this work. Combining the information from published works, a good starting point for creating analogs of BFP is through derivatization of the C4, C7 and C8 positions. In addition, the C2 site serves as an interesting position since, to the best of the author's knowledge, no previous work investigated that specific part of the BFP core.

To further decide which substituents have potential to increase the affinity of the ligands to enzyme's binding pocket, the Topliss decision tree was utilized. This decision parameter is a tool used in drug discovery to suggest substituents combining hydrophobicity, mesomeric, electronic, and steric effects in the design of analog compounds. In this work, the attachment of either alkyl chains, or aromatic groups substituted with either electron donating/withdrawing groups at various positions was guided by the Topliss parameters. For example, the unsubstituted phenyl ring was used first (in all series) as a base substituent followed by attaching either electron-donating or -withdrawing groups at varying positions in the ring, patterned from the design of the tree parameters. Therefore, the tree was utilized to rationalize the observed substituent effects and guide the exploration of other chemical moiety/appendages but did not solely dictate the final set of designed BFP derivatives.

Lastly, to provide an actual jump board on the preparation of derivatives, a preliminary docking of the unsubstituted 2,6-dhBFP to the binding pocket of CDK-5 *(see Figure **S1**)* was conducted. The results revealed that the docking of the said ligand exhibited very few interactions with the amino acids in the active binding site of CDK-5, signaling that the core BFP moiety requires derivatization by adding structural appendages that will eventually increase the number of interactions between the ligand and the active site. Moreover, the 3D-visualization of the docking showed that the binding pocket is hollow and the interactions between the ligand and the specific amino acids are also distant *(Figure **S1a** and **S1b**)*, prompting a possible substitution of larger moieties such as the aromatic phenyl ring. Considering the three parameters listed above for the derivatization strategy, this study concentrated on developing BFP derivatives with a maintained 6-OH group, having variable substitutions at the C4-position (**B**1-**X**-1 series) and the C7/C8-positions (**B**1-1-**X** series). Moreover, to provide a comprehensive investigation of the BFP core, this work explored varying the substituents at the C2-position rather than the C3-position, resulting in the **BX**-1-1 series, which could offer more insights into future protocols for BFP analogs synthesis. The structure of the 104 BFP derivatives is listed in Figure 3.

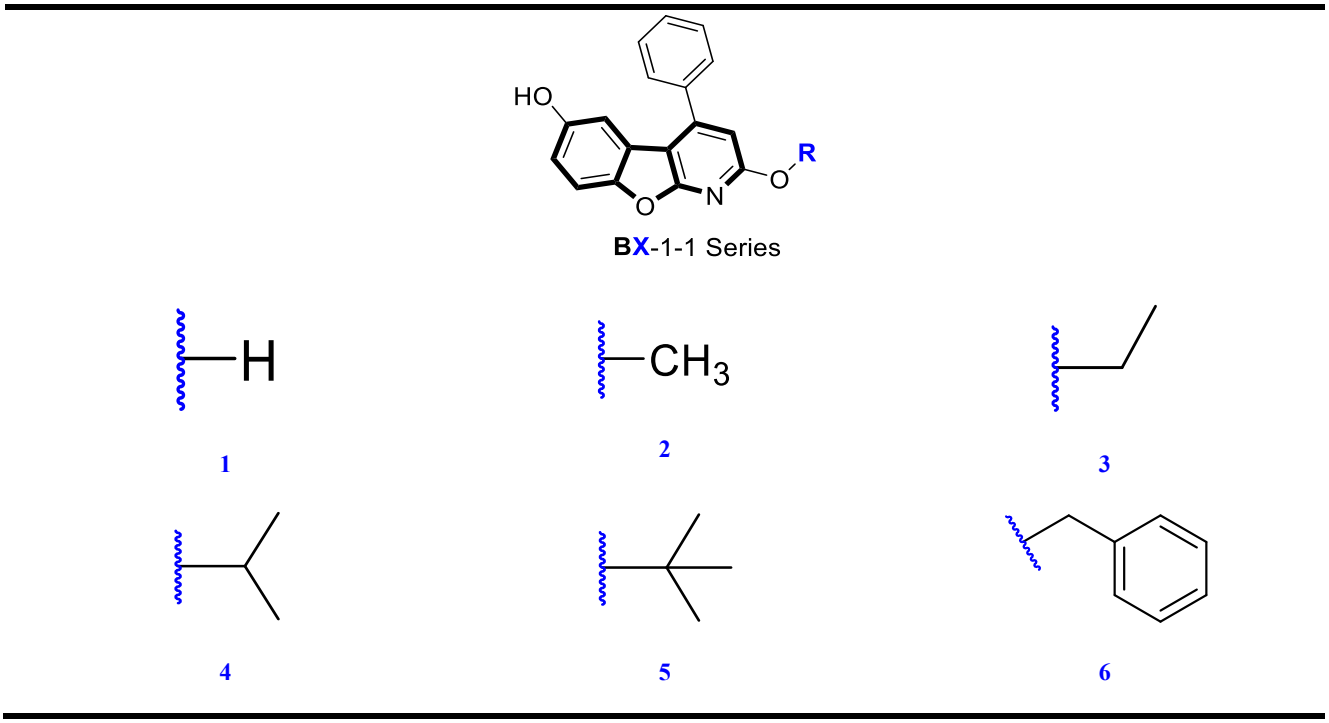

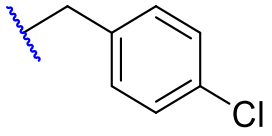

7

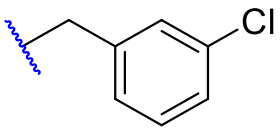

8

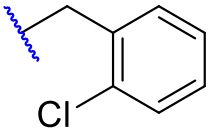

9

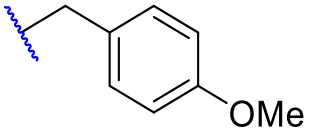

10

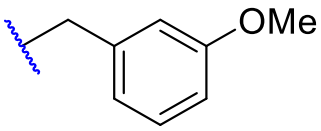

11

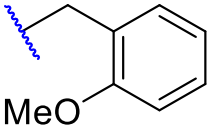

12

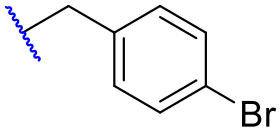

13

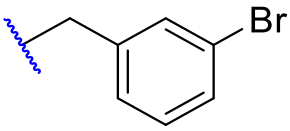

14

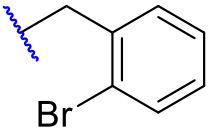

15

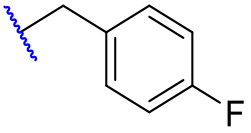

16

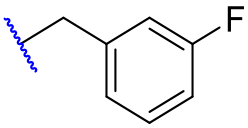

17

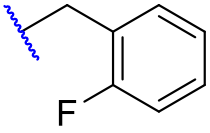

18

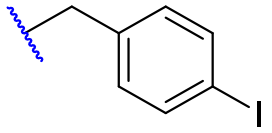

19

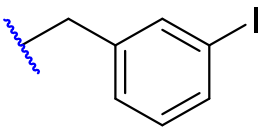

20

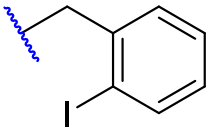

21

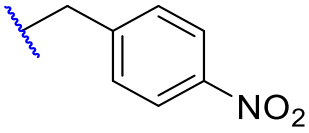

22

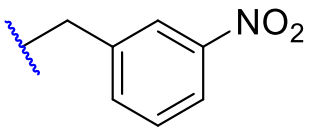

23

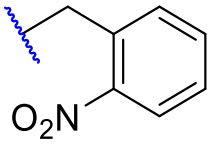

24

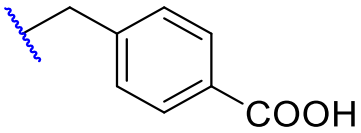

25

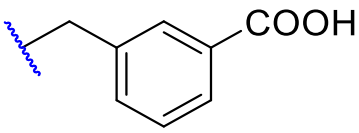

26

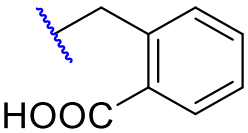

27

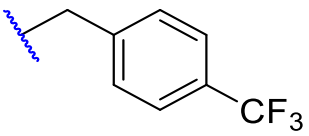

28

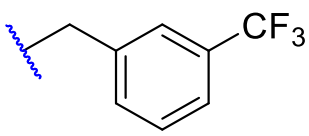

29

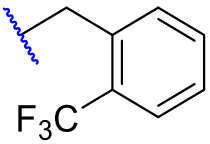

30

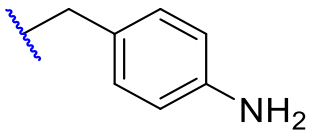

31

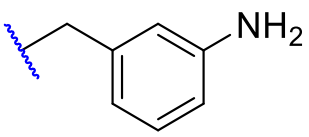

32

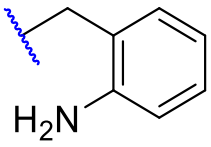

33

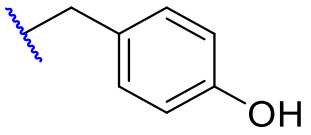

34

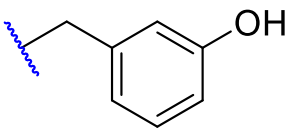

35

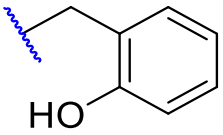

36

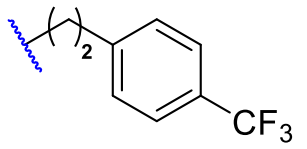

37

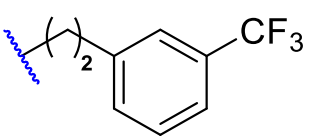

38

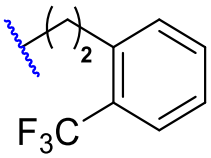

39

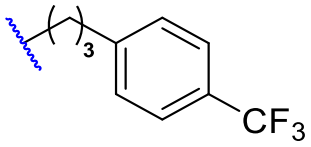

40

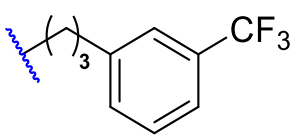

41

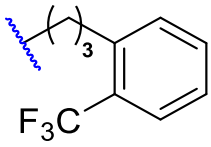

42

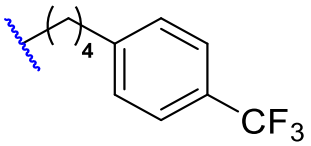

43

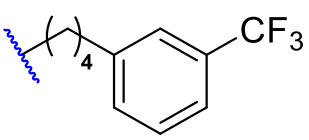

44

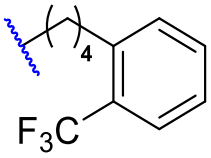

45

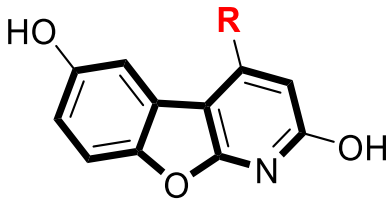

B1-**X**-1 Series

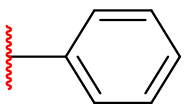

1

2

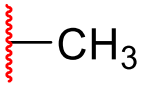

3

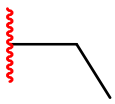

4

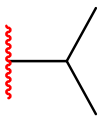

5

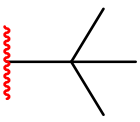

6

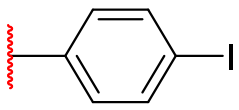

7

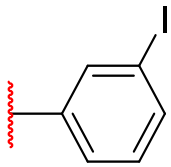

8

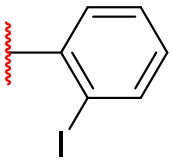

9

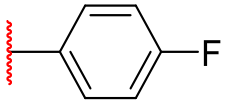

10

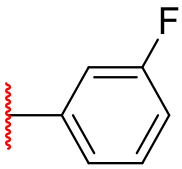

11

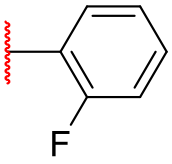

12

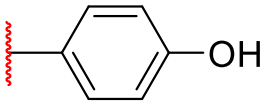

13

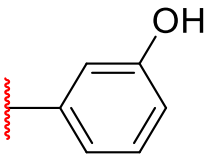

14

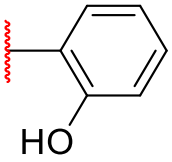

15

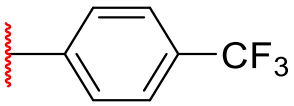

16

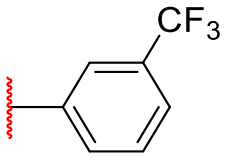

17

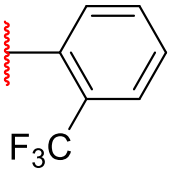

18

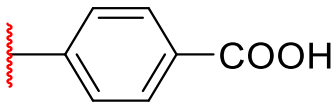

19

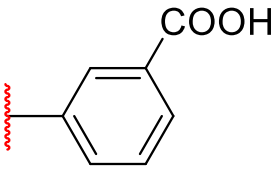

20

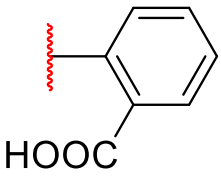

21

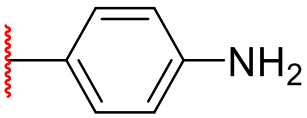

22

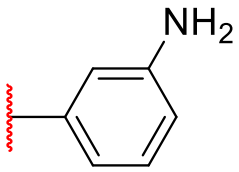

23

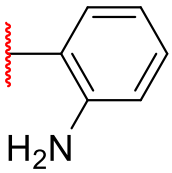

24

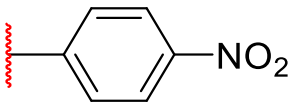

25

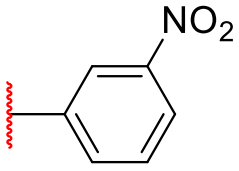

26

27

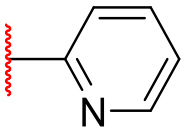

28

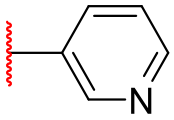

29

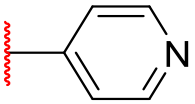

30

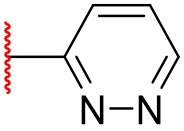

31

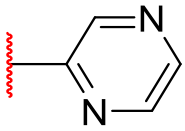

32

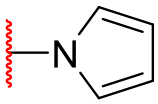

33

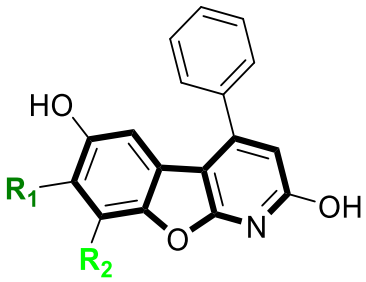

B1-1-**X** Series

R_1 = H, R_2 = H

1

R_1 = Br, R_2 = H

2

R_1 = I, R_2 = H

3

R_1 = F, R_2 = H

4

R_1 = Cl, R_2 = H

5

R_1 = NH_2, R_2 = H

6

R_1 = NO_2, R_2 = H

7

R_1 = COOH, R_2 = H

8

R_1 = CF_3, R_2 = H

9

R_1 = H, R_2 = Br

10

R_1 = H, R_2 = I

11

R_1 = H, R_2 = F

12

R_1 = H, R_2 = Cl

13

R_1 = H, R_2 = NH_2

14

R_1 = H, R_2 = NO_2

15

R_1 = H, R_2 = COOH

16

R_1 = H, R_2 = CF_3

17

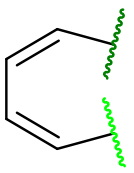

18

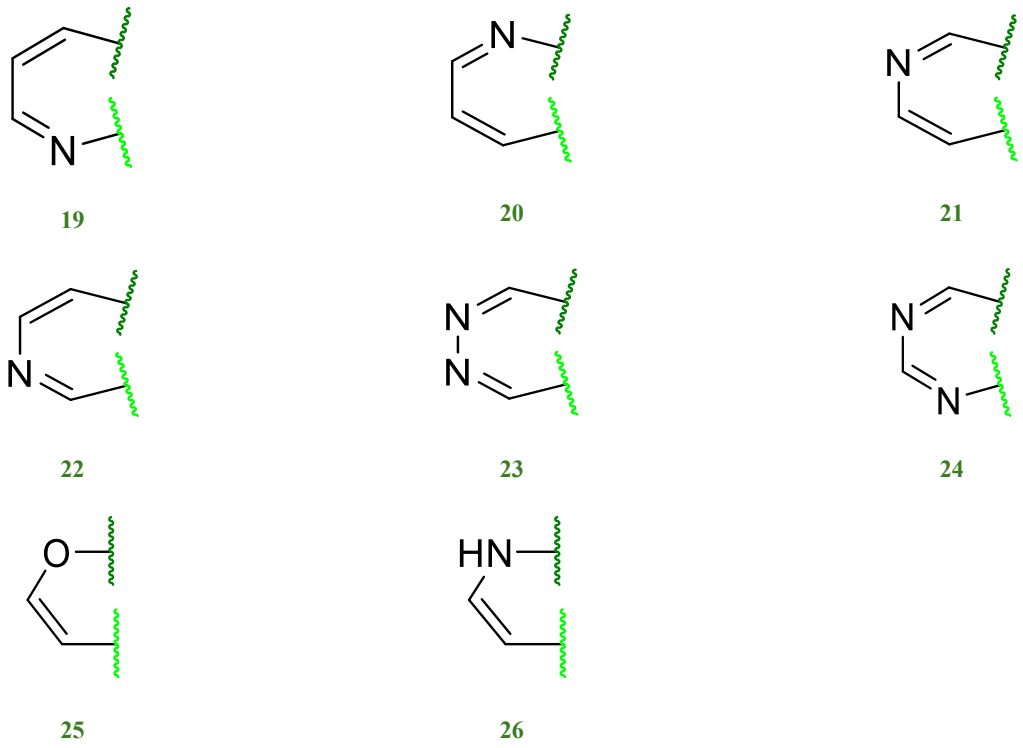

Figure 3: Structure of the BFP derivatives in the three optimization series: **B**X-1-1 (45 compounds), **B**1-X-1 (33 compounds) and **B**1-1-X (26 compounds)

Molecular Docking Analysis

Method Validation

To assess the quality and the precision of the docking method, a validation study was conducted using the re-dock strategy. Roscovitine (RSC), the co-crystallized ligand from the PDB structure of the CDK-5 enzyme, was isolated. The structure was redrawn and was subjected to the docking method described in this study. The redrawn ligand was then overlaid with the original co-crystallized RSC in the active site of the enzyme. The overlaid structures of roscovitine are presented in Figure 4. As shown, both the original co-crystallized RSC and the redrawn ligand docked using the method in this work were smoothly overlapping with each other. This finding provides a good approximation of the accuracy and precision of the docking method in this work, as compared with the x-ray crystallization method used in the actual PDB file of the kinase enzyme. To further validate the qualitative overlay of the co-crystallized and re-docked RSC, the Root Mean Square Deviation (RMSD) value was determined resulting in 1.506 angstrom (Å) which falls within the acceptable limit of less than or equal to 2.0 Å, a widely known threshold in redock strategies (Kramer et al. 2008).

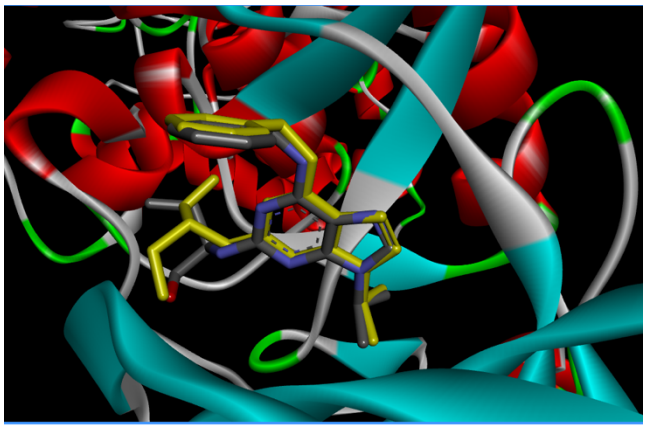

Figure 4: Overlay of two roscovitine structures; co-crystallized ligand from Protein Data Bank (in yellow) and the redrawn compound (in gray) at the active site of CDK-5.

BX-1-1 Series

This group of BFP analogs investigated the potential of derivatizing the 2-OH position, which, to the best of the author's knowledge, has not been explored previously. A total of 45 derivatives were prepared incorporating diverse substituents, including alkyl group of varying sizes, and 2-O-benzyl groups bearing halogen, amino, carboxyl, and other functional attachments. These substituents were placed at either ortho-, para-, and meta-positions with respect to the 2-O site. To elucidate the effect of linker lengths, compounds **37** to **45** of the **B**X-1-1 were prepared *(as shown in a separate graph, Figure 5)* by modifying the number of methylene (-CH_2) groups attached to the trifluoromethylbenzyl substituent, adding 2-3 more carbons in the chain. The summary of the binding affinities of the **B**X-1-1 series with its *in silico* structure-activity relationship (SAR) is presented in Figure 5.

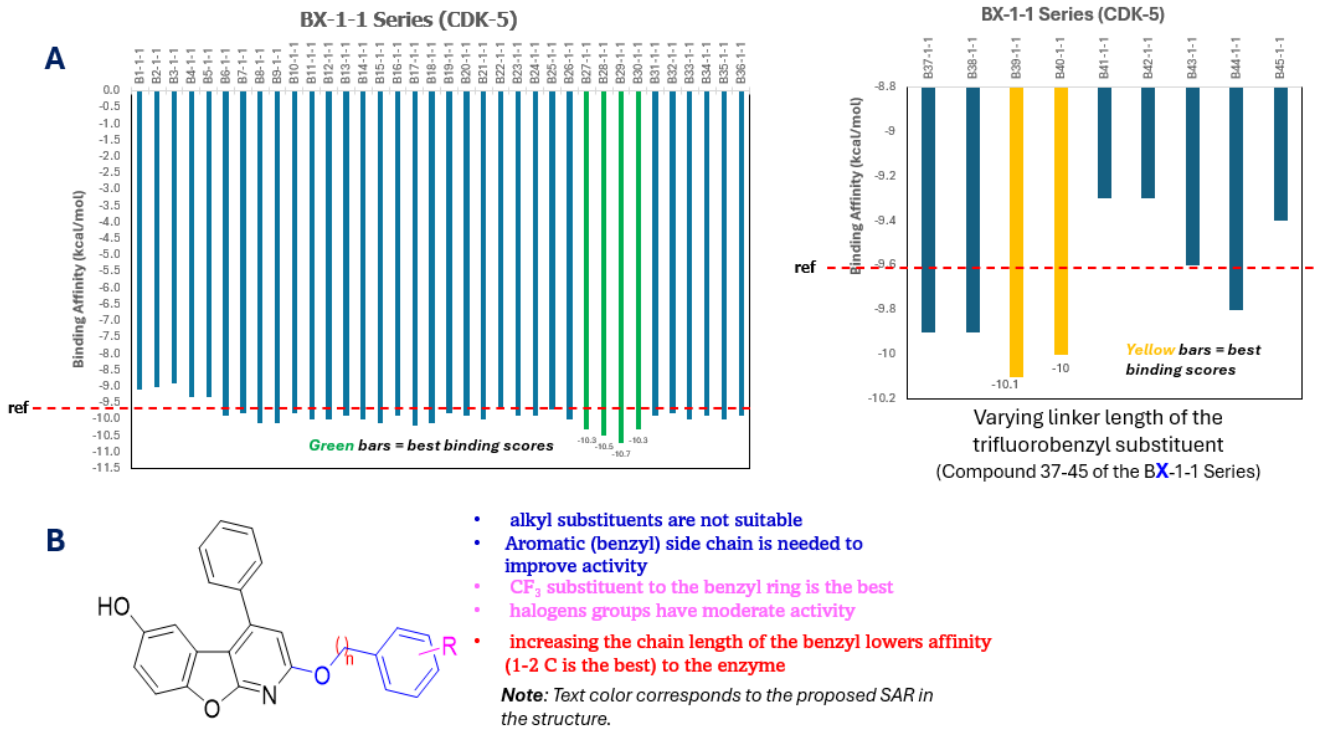

Figure 5: (**A**) Binding affinities of the **B**X-1-1 series (45 analogs) to the CDK-5 enzyme; **ref** as the baseline compound in red dotted line. Compound **B**37-1-1 to **B**45-1-1 varies the (-CH_2) chain length of the trifluoromethylbenzyl substituent. (**B**) Summary of the structural optimization for the proposed SAR of this series.

The results of the molecular docking revealed that the majority of the analogs improved their binding energy as compared to the **ref** upon substituting the C2 position. The binding energy (docking score) is a measure of interaction between the target site of the enzyme with the respective ligand, in which a more negative binding energy (in kcal/mol) means that the ligand is more attracted to the active site (Agu et al. 2023). It is obvious in the data that the benzyl group has the best result with the trifluoromethyl (-CF_3) substituent as the best attachment to the ring as proven by **B**28-1-1, **B**29-1-1 and **B**30-1-1 (*see Table 1*) compounds. It is also worth noting that alkyl substituents seemed to be unfavorable groups to be attached in the 2-O region of the BFP. Compounds 37 to 45 of the **B**X-1-1 series explored the effect of the methylene linker length on the binding affinity with the assumption of a possibility to push the ligand near the interacting amino acids in the active site. However, the results revealed that extending the carbon chain length up to three or more -CH_2 (derivative 41 to 45 of the **B**X-1-1 series) has a negative effect on the docking score, while confirming that having one methylene attached to the trifluoromethylphenyl substituent is still the best group in this series.

B1-X-1 Series

In this series, the C4 position of the BFP was investigated for possible improvement of the binding affinity to the CDK-5 enzyme. The results of this optimization series are summarized in Figure 6. As shown in the plot, truncating the 4-phenyl group from BFP, resulting in the **B**1-2-1 analog, greatly lowered the binding energy to -7.6 kcal/mol which highlighted the importance of the benzene ring in the C4 site as reported in previous literature. This is also consistent with the observations in the preliminary docking (*Figure S1*) where a bulky group is necessary to compensate the hollow active site of the CDK-5 when docked with 2,6-dhBFP. The docking study also revealed that replacing the benzene ring with heteroaromatic groups like pyridine, diazine and pyrrole rings does not have much effect on improving the docking score (**B**1-28-1 through **B**1-33-1; 6 compounds).

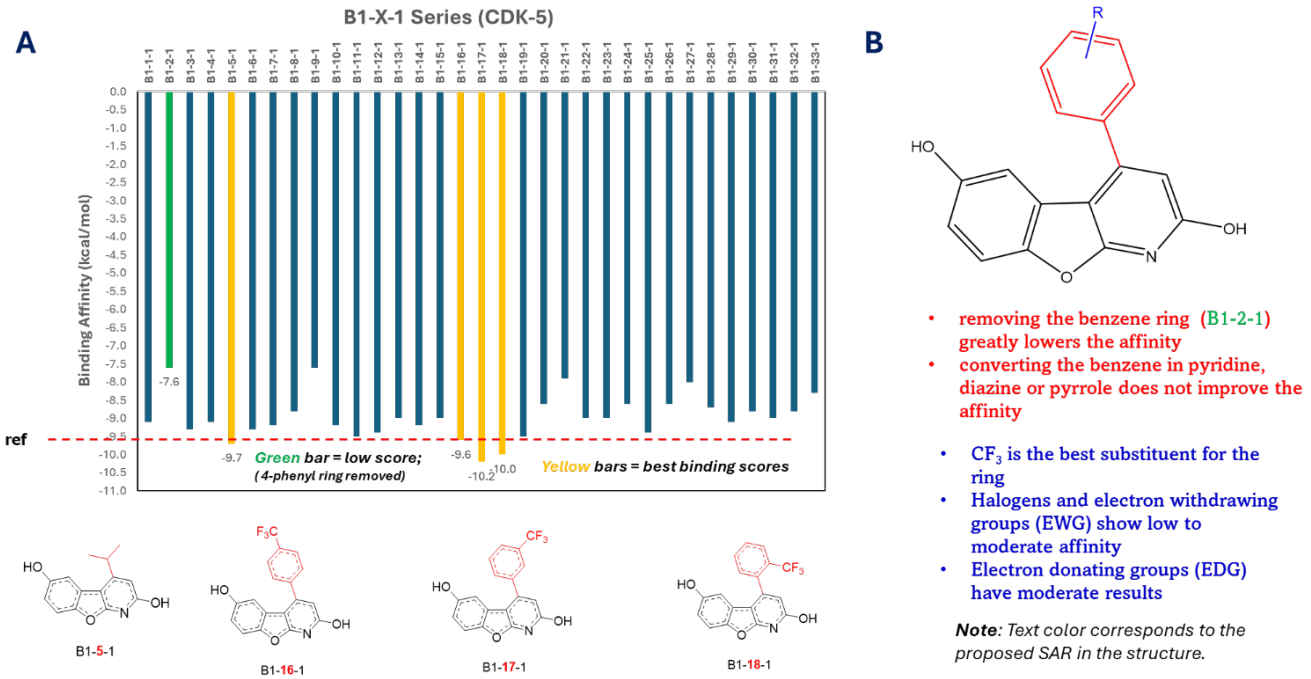

Figure 6: (**A**) Binding affinities of the **B**1-**X**-1 series (33 analogs) to the CDK-5 enzyme and the structure of the best analogs; **ref** as the baseline compound in red dotted line. (**B**) Summary of the structural optimization for the proposed SAR of this series.

It is interesting that the trifluormethyl (-CF_3) substituent is also the best attachment to the 4-phenyl ring, consistent with the results of the **BX**-1-1 series. Moreover, attaching an isopropyl group to the C4 position positively increases the binding energy of the BFP to the CDK-5 as shown by **B**1-**5**-1 analog, which is slightly better as compared to the **ref** compound.

B1-1-X Series

This optimization series focused on the benzene side of the BFP which explored the addition of groups specifically at the C7 and/or C8 sites of the core compound. A total of 26 derivatives were prepared and the summary of the results with the *in silico* SAR is shown in Figure 7.

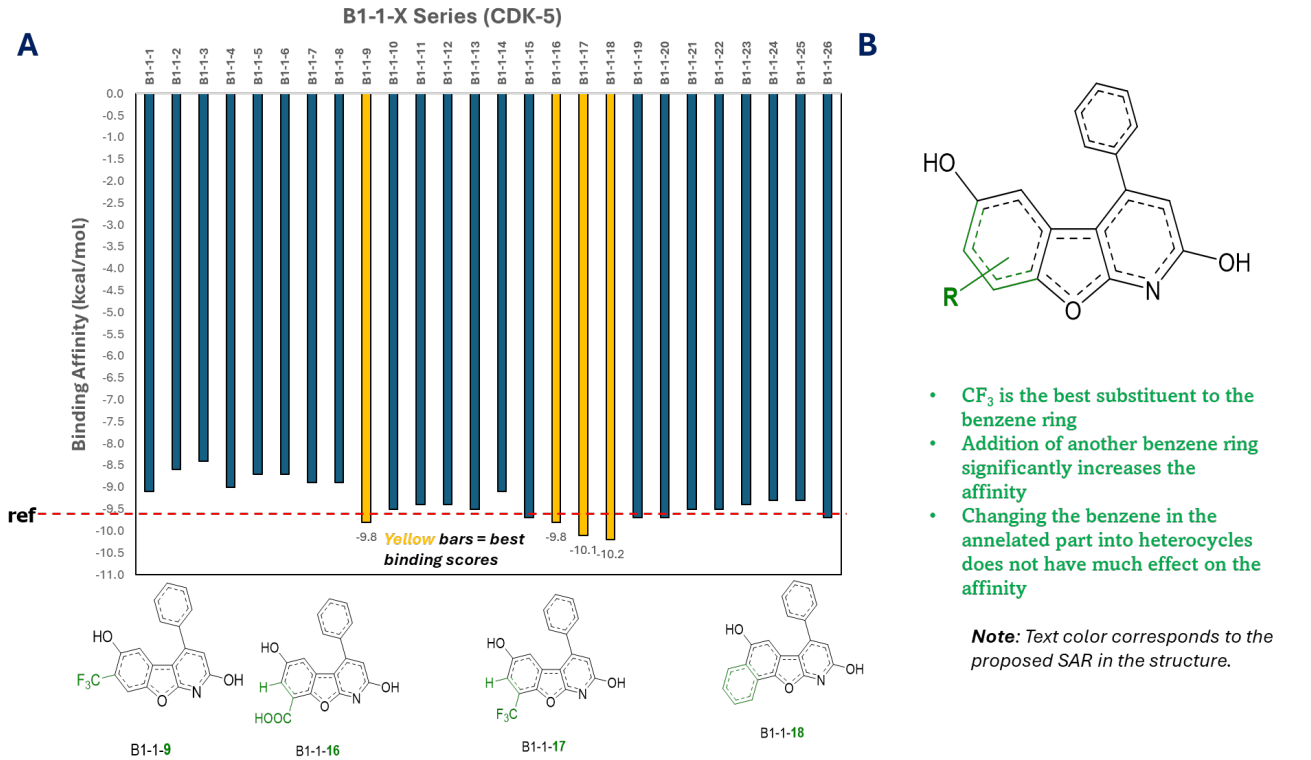

Figure 7: (**A**) Binding affinities of the B1-1-**X** series (26 analogs) to the CDK-5 enzyme and the structure of the best analogs; **ref** as the baseline compound in red dotted line. (**B**) Summary of the structural optimization for the proposed SAR of this series.

The results demonstrated that the addition of groups (halogens, NH_2, COOH, etc.) at the C7 position did not significantly increase the binding energy as compared to the **ref** compound, except when CF_3 (**B**1-1-**9**) was attached. Conversely, adding those substituents in the C8 position especially the trifluoromethyl and the carboxylic group (**B**1-1-**16** and **B**1-1-**17**) dramatically improved the docking score. In addition, annelating another benzene ring resulting in the **B**1-1-**18** derivative, increases the affinity of the BFP by approximately 0.6 kcal/mol (-10.2 kcal/mol) as compared to the **ref**. This result is consistent with the findings of Holzer et al. (Holzer et al. 2018) (*see Figure **1d***) highlighting the importance of the annelated benzene group, with this work introducing a new

structural feature: modification of the 2-OH rather than the 3-OH site.

Summary and 2D Visualization

The binding energies of all the 104 BFP derivatives were plotted and presented in Figure 8 *(see Table **S1-S3** for the listing of the compounds with their binding scores)*.

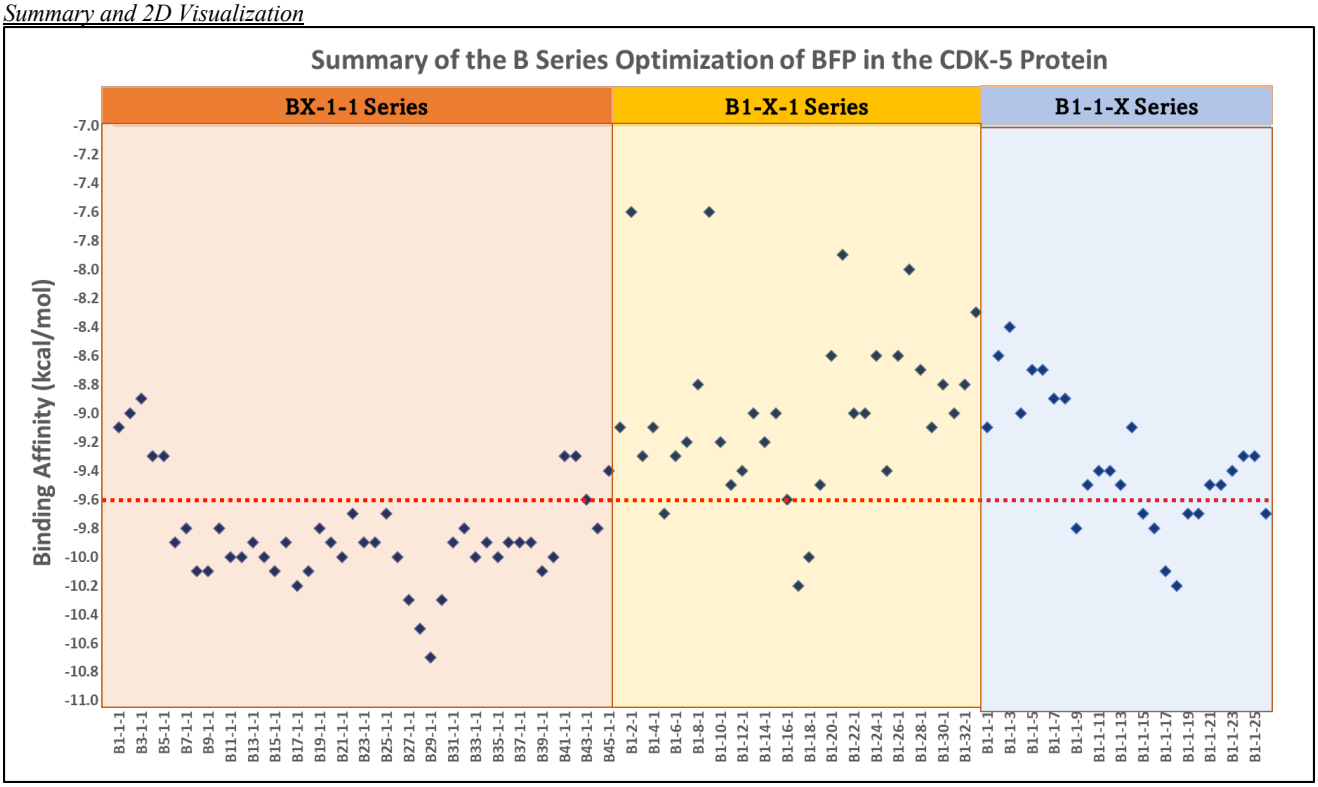

Figure 8: Summary plot of all analogs across the three structural optimization series of the BFP moiety and their binding energies with the CDK-5 enzyme. Red dotted line is the binding energy of the **ref** compound.

It is evident that among the three optimization plans, the **BX**-1-1 group exhibited the highest potential for future derivatization. As shown in Figure 8, thirty-seven (37) out of the 45 analogs in that series have better docking score as compared to the reference compound (***ref***). This proves the likelihood of the C2 position of the BFP to be functionalized to produce more potent inhibitors against CDK-5 and its related pathologies. These observations are in consonance with the outcomes of the author's previous work (Ereje et al. 2025), where novel BFP derivatives were synthesized and were characterized concentrating on substituting the 2-O position only, producing analogs which are potent against a variety of cancer cell lines. In contrast, it seems that the **B**1-**X**-1 series has the least derivatization potential with only 3 compounds having better affinity compared to the **ref**, which again corroborates that the 4-phenyl ring of the BFP is an important substituent and must be retained to maintain the activity against CDK-5. Moreover, the last series **B**1-1-**X** produced some better analogs while confirming previous results on the importance of the phenyl-annelation in the BFP core.

Nine BFP derivatives, three from each optimization series, were chosen to be representative BFP ligands for further investigation of their potential as CDK-5 inhibitors and future drug candidates. The choice of these ligands was mainly due to their high binding scores as compared to the **ref** compound, and including other important parameters such as structural diversity, the type or electronic effects of substituents, and information from previous studies. Ligands **11**, **27**, and **29** from the **BX**-1-1 series; **2**, **11**, and **17** from the **B**1-**X**-1 series; and **9**, **17**, and **18** from the **B**1-1-**X** series were selected as representative BFP compounds. Although **B**1-**2**-1 exhibited low binding energy during the docking simulation, it was retained for analysis to evaluate the structural effects of truncating the 4-phenyl substituent of the benzofuropyridine core. Previous literature establishes this specific appendage as a critical pharmacophoric determinant for CDK-5 binding affinity. Additionally, **B11**-1-1 was selected due to its structural homology to a synthesized benzofuropyridine (BFP) derivative known for potent anticancer activity. Conversely, despite its favorable binding score, **B**1-1-**16** was excluded from further analysis because its predicted affinity was identical to that of **B**1-1-**9**. Moreover, **B**1-1-**9** was prioritized to further investigate the effects of varying -CF_3 position in the C7 and C8 position of the BFP core structure.

To better understand the binding score of these analogs, the two-dimensional (2D) interaction of the ligands with the CDK-5 target binding site was visualized and presented in Figure S2.

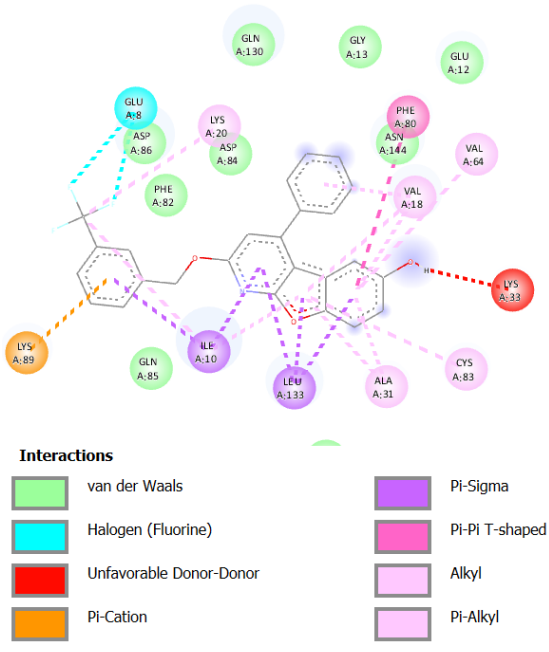

Figure 9: Two-dimensional (2D) visualization of **B29**-1-1 ligand in the binding pocket of CDK-5 enzyme.

The features of CDK-5 enzyme, especially its active binding site, provide a better understanding of its potential bioactivity with emphasis on related pathologies of known diseases such as Alzheimer's (Liu et al. 2015), and even cell cycle regulation in cancer (Xie et al. 2016; Meder et al. 2016; Wei et al. 2016). As shown in Figure S2, key interactions of the representative ligands with important amino acid residues were identified. For example, Phenylalanine 80 (Phe80) also known as the gatekeeper amino acid (Lenjisa et al. 2017), exhibited pi-pi T-shaped interaction with the benzene moiety of the core BFP in most of the ligands. This observation is also noticeable with the same interaction presented by the annelated Benzene ring in **B**1-1-**18**. Moreover, a pi-alkyl interaction was formed with Phe80 and BFP upon addition of the CF_3 substituent as demonstrated in **B**1-1-**9** and **B**1-1-**17**. The gatekeeper amino acid is an important residue especially in maintaining access to the hydrophobic portion of the CDK-5 active site.

Another crucial residue is Cys83 which is located in the hinged region (Lenjisa et al. 2017) of the enzyme, responsible for properly orienting ATP (Adenosine Triphosphate), the source of phosphate group in the catalytic activity of kinases where CDK-5 belong. It is worth mentioning that the lead compound **B29**-1-1 having the highest binding affinity of -10.7 kcal/mol among the 104 derivatives, have shown a pi-alkyl type of interaction with Cys83, a pi-pi T-shaped interaction with Phe80, and pi-cation binding with Lys89 leading to its strong stability in the CDK-5 pocket as presented in Figure 9. To visualize and investigate it better, the actual 3D active site pocket of CDK-5 with the docked **B29**-1-1 ligand is shown in Figure 10.

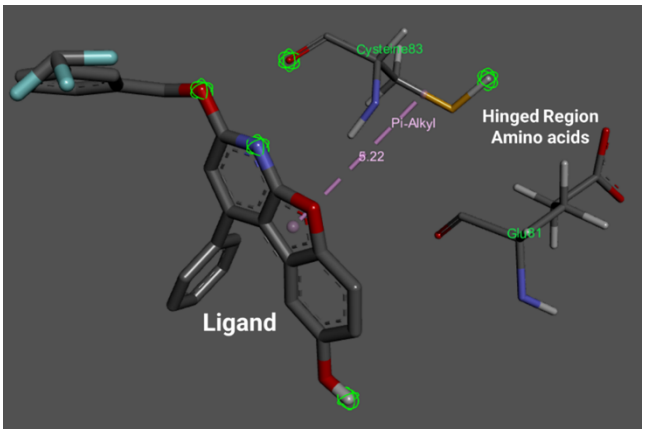

Figure 10: Three-dimensional (3D) visualization of the docked **B29**-1-1 in the CDK-5 binding pocket. Green spheres in the structure are identified molecular pharmacophores.

The hinged region amino acids were presented in the 3D view to investigate the position of the ligand with respect to key residues in the binding pocket. In Figure 10, it was seen that the length of the pi-alkyl interaction between the ligand and Cys83 is approximately 5.22 angstrom which is a bit longer to standard 4.0 angstrom distance for significant interaction strength. This provides the potential of further functionalizing the molecular scaffold to shorten the distance creating other interactions especially to another hinged region residue, Glu81, known for inducing selectivity to CDK-5 as compared among other CDKs. In addition, three atomic positions in the **B29**-1-1 ligand were considered as potential pharmacophores, sites where possible new interactions can be designed to improve biological activity. The 2D visualization of the docking study revealed that a conventional hydrogen bond (H-bond) interaction exists between Cys83 and the oxygen in the furan ring of the BFP. Interestingly, the interaction with Cys83 and the BFP ligands disappeared upon removing the 4-phenyl group as seen in **B**1-**2**-1 that could explain its poor binding score result, again highlighting the importance of the 4-phenyl group in maintaining the supposed bioactivity against CDK-5. Conversely, unfavorable interactions were also found with key amino acids such as Glu81 (another hinged region residue) in **B**1-**2**-1, Cys83 in **B**1-**11**-1, Lys33 with **B**1-1-**9** and **B**1-1-**18**, explaining their lowered binding score which validated why the **BX**-1-1 series might be the most logical derivatization plan to pursue in the actual synthesis of BFP analogs as inhibitors of CDK-5.

Physicochemical and ADME Properties Prediction

To investigate further the potential of the identified BFP analogs as future candidate molecules for drug discovery, their physicochemical and ADME (Doogue and Polasek 2013) properties were predicted and examined. The representative BFP (including **B**1-**2**-1) compounds were analyzed using the SwissADME (Daina et al. 2017), a free software for predicting drug-likeness of molecular scaffolds. The predicted parameters of the 9 BFP representative derivatives are summarized in Table 1.

Table 1: Physicochemical and ADME properties of representative BFP analogs from the three optimization series.

Compound Code	Physicochemical Properties				Lipophilicity	Solubility	Pharmacokinetics		Druglikeliness		Medicinal Chemistry	
	Molecular Weight (g/mol)	No. of H-bond acceptors	No. of H-bond donors	Topological Polar Surface Area (Å^2)	Log Po/w	Solubility Class	CYP1A2 Inhibitor	CYP2C19 Inhibitor	No. of Violations (Lipinski Rule)	Bioavailability Score	PAINS Alert	Synthetic Accessibility
B11-1-1	397.42	5	1	64.72	4.85	Poorly soluble	Yes	Yes	0	0.55	0	3.69
B27-1-1	410.4	6	1	95.62	4.08	Poorly soluble	No	Yes	0	0.56	0	3.54
B29-1-1	435.39	7	1	55.49	5.9	Poorly soluble	Yes	Yes	1	0.55	0	3.62
B1-2-1	201.18	4	2	66.49	1.96	Soluble	Yes	No	0	0.55	0	2.53
B1-11-1	295.26	5	2	66.49	3.62	Moderately soluble	Yes	Yes	0	0.55	0	2.87
B1-17-1	345.27	7	2	66.49	4.26	Moderately soluble	Yes	Yes	0	0.55	0	3.04
B1-1-9	345.27	7	2	66.49	4.21	Moderately soluble	Yes	Yes	0	0.55	0	3.07
B1-1-17	345.27	7	2	66.49	4.32	Moderately soluble	Yes	Yes	0	0.55	0	3.12
B1-1-18	327.33	4	2	66.49	4.21	Moderately soluble	Yes	Yes	0	0.55	0	3.14

The 9 BFP derivatives demonstrated low (<150) Topological Polar Surface Area (TPSA), a parameter which measures the molecule's surface area with respect to its polar atoms which is highly related to the drug's bioavailability (Prasanna and Doerksen 2009) and permeability. In addition, they did not violate the Lipinski Rule (Daina et al. 2017) for drug-likeness, and all their bioavailability scores were around 0.55, indicating potential stability and permeability. In terms of their Medicinal Chemistry, all analogs were not flagged as PAINS (Baell and Holloway 2010), or those molecules that usually present false-positive results in screenings and assays (Baell and Nissink 2018). Moreover, their Synthetic Accessibility score (Ertl and Schuffenhauer 2009) are all less than 3.70 revealing the relative ease of the synthetic procedures for the analogs (a score of **1** indicates easy synthesis, while **10** indicates difficult synthesis), should they be produced for laboratory (*in vitro*/*in vivo*) testing. The ADME parameters of **B29**-1-1 are all within acceptable values (*Table 1, highlighted in red*) except for its poor solubility which was also flagged as a violation in the Lipinski rule. Alternatively, **B**1-**11**-1 and **B**1-1-**18** (*Table 1, highlighted in blue*) from the other two series, can also be considered for future drug design as they exhibited excellent predictive ADME results including better solubility as compared to **B29**-1-1.

Lastly, to predict both the permeability of the compounds through the Blood-Brain Barrier (BBB), and their Human Gastrointestinal Absorption (HIA), the **BOILED-Egg** (**B**rain **O**r **I**ntestina**L** **E**stimate**D** permeation) (Daina and Zoete 2016) predictive model was generated. The results are presented in Figure 11.

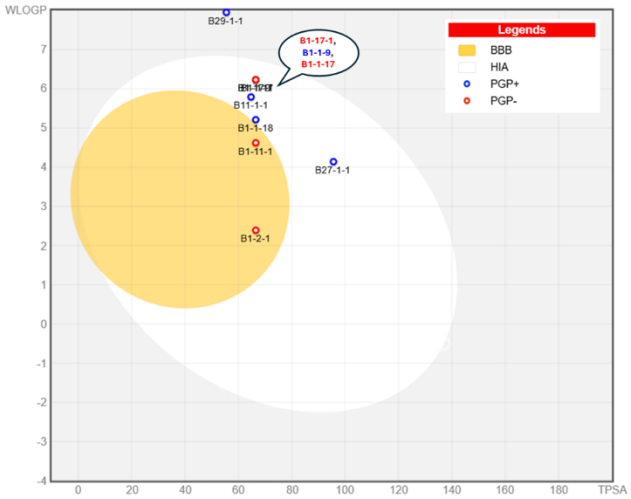

Figure 11: Boiled-egg analysis of the 9 representative BFP analogs from each optimization series.

The results showed that among the BFP representative compounds, two derivatives, namely **B**1-**2**-1 and **B**1-**11**-1 (yolk region), exhibited the potential to permeate the BBB freely and to access the Central Nervous System (CNS). This finding is crucial as the study is focusing on CDK-5 enzyme, which is mainly found in post-mitotic neurons, thus making BBB permeation an important consideration for these derivatives to become effective future drug candidates. The results of the BOILED-Egg highlight the potential of **B**1-**11**-1 to be a future drug candidate since it can freely pass through the BBB. As a PGP- analog (red dot), the compound is not easily excreted out of the compartment revealing its potential high retention in the brain. **B**1-1-**18**, the phenyl-annelated BFP, also exhibited high binding score as well as potential for BBB permeation since it near the border of the yolk region, prompting possible structural modifications to improve absorption. Six other representative compounds were predicted to be passively absorbed in the gastrointestinal (GI) tract as represented by the egg-white region of the model. It is important to note that in the BOILED-Egg, the permeation in either the BBB or GI are not mutually exclusive.

Interestingly, **B29**-1-1 is the only compound outside the "egg" portion revealing its poor possibility to be absorbed, that can be explained by its high lipophilicity and large molecular mass which was flagged as well in the Lipinski prediction. Since **B29**-1-1 is among the best compounds with the highest binding score, BBB

permeation might be a crucial obstacle in developing the analog as a CDK-5 inhibitor. However, given the predictive SAR of the derivatization series, one possible fix to the high molecular weight and lipophilicity of **B29**-1-1 is to truncate the 4-phenyl substituent to be replaced by smaller alkyl groups such the isopropyl moiety, inspired from the result of B1-**5**-1 with binding affinity of -9.7 kcal/mol. Another possible solution is to remove the phenyl ring in the 2-O position of the BFP, replacing it with a methylenetrifluoromethyl (-CH_2CF_3) group. This is in consonance with the SAR presented by the **BX**-1-1 series which highlights -CF_3, attached via a single -CH_2 linker, as one of the best substituents at the C2 position of the core BFP. The two alternatives presented will make sure to maintain the high affinity of **B29**-1-1 against CDK-5 while addressing issues on structural limitations resulting in poor BBB permeation as informed by the results of the BOILED-Egg analysis.

Another important piece of information from this model is the prediction whether the compounds can be potential substrates of the P-glycoprotein (PGP), an active efflux system that flushes out materials from the brain or to the GI lumen (Lin and Yamazaki 2003). As shown in Figure 11, four derivatives (including all representative analogs in the **B**1-**X**-1 series) are PGP- substrates, highlighting their ability to be retained longer in physiological compartments and not easily secreted out; while all the other compounds, mostly the GI-absorbed group, are PGP+, which poses a problem especially regarding their bioavailability and expected potency.

Molecular Dynamics (MD) Simulation

To further study the interaction of the protein and the ligand complex through time, a molecular dynamics simulation was performed with the highest binding score ligand **B29**-1-1 and CDK-5 using standard protocols and procedures. The results were visualized and the data are presented in Figure 12.

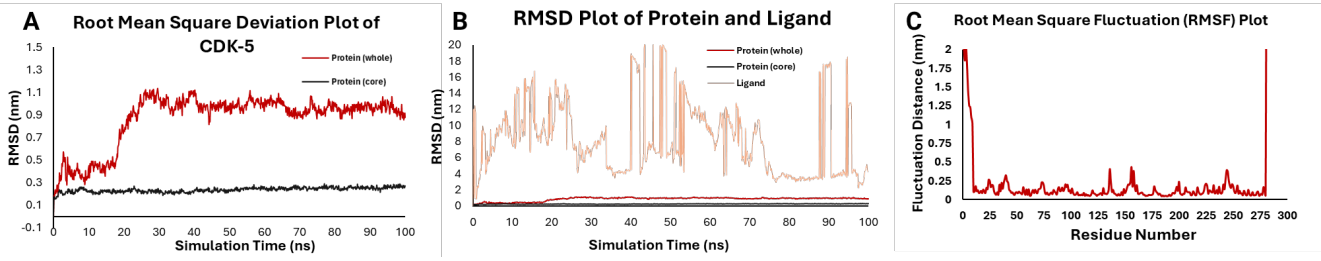

Figure 12: Results of the MD Simulation of **B29**-1-1 with CDK-5. (**A**) RMSD plot of protein only. (**B**) RMSD plot of the protein overlaid with the ligand. (**C**) RMSF Plot of the system.

In Figure 12A, the analysis of the whole protein sequence (represented in red) and the truncated core enzyme lacking the N- and C-terminal residues (represented in black) both demonstrated structural stabilization over a 100-nanosecond time scale, as confirmed by their RMSD values. Moreover, even though both results fall within acceptable limits, a reduction in RMSD was observed upon truncating the terminal residues, confirming the steadiness and efficient folding of the important core residues. These observations were corroborated by the RMSF plot (Figure 12C) showing an erratic and unsteady movement of residues 1-10, and residues above 280 having very high fluctuation.

Even though the protein structure exhibited stability, the ligand results revealed otherwise. As seen in Figure 12B, the ligand has not stabilized during the 100 ns simulation run. The results showed signs of equilibration and dramatic reduction of RMSD at around 80 ns but reached some high peaks at 90 and 95 ns mark. This result suggests that the ligand may take time to stabilize with the protein, thus, a longer simulation run, extended up to 200–500 ns, may be needed to better visualize the performance of **B29**-1-1 in the MD simulation.

The result in the RMSF plot in Figure 12C also provides indicative information that may explain the behavior of the **B29**-1-1 ligand in the MD study. Specifically, the peak point at residue 155 in the RMSF plot highlights significant motion and fluctuations. This region of the CDK-5 is known to be part of the T-loop or activation loop (residue 145-172), which controls access to the active site of the enzyme. The T-loop is known to be highly flexible, and the flapping of those residues may have potentially pushed the ligand out of the binding pocket explaining the high RMSD values. Another key RMSF peak is the one from residue 40, which is part of the Glycine-rich region or the P-loop which controls ATP coordination. The high fluctuation distance peak in this residue suggests that the binding pocket may have been turning on and off entry of molecules preventing the ligand to acclimatize into a more relaxed pose. Given that the RMSD and the RMSF analyses were sufficient to explain the protein-ligand interactions, other standard MD metrics like binding free energy and radius of gyration were not presented in detail. In addition, while the results of the molecular dynamics simulation indicate the instability of **B29**-1-1 in the CDK-5 active site, further investigation is necessary to accurately identify the potential bioactivity of the ligand to the target protein. Actual synthesis of the ligand and various *in vitro* or *in vivo* tests, such as enzyme inhibition and kinetics studies, are essential to validate computational data.

Future Synthetic Direction

Combining the molecular docking and ADME prediction, the results suggest which potential BFP analogs have high affinity to CDK-5, their possible substitution pattern, and their probable sites of derivatization for future design. For example, the **B11**-1-1 analog emerged to be one of the top-performing compounds in this study, building upon the author's previous work (Ereje et al. 2025) where a related BFP derivative was synthesized (*compound **3c***) having a similar structure to **B11**-1-1 except for the 4-phenyl group. The comparison further corroborates the result on the likelihood of the 2-O position for future BFP drug design. In that mentioned work, **3c** exhibited potent activity against various cancer cell lines possibly related to CDK-5 pathology, which emphasizes the importance of the use of computational tools in conjunction with actual molecular synthesis to produce candidate CDK-5 inhibitors and effective treatment regimens.

CONCLUSION

Three derivatization series were planned, concentrating on the C2, C4, and C7/C8 positions of the BFP core structure. Substitution patterns were optimized for possible CDK-5 inhibition using molecular docking studies and ADME predictions. A total of 104 analogs were prepared and docked to the enzyme's active site. The binding affinities were analyzed and key structural distinctions were summarized producing 3 representative compounds from each series as future drug candidates. Important amino acid residues and their specific interactions with the 9 ligands were further investigated to provide insight into the supposed bioactivity

of the BFP analogs as CDK-5 inhibitors. Drug likeliness and other molecular parameters were also predicted using SwissADME, offering a more cohesive understanding of the relationship between the substitution of the BFP and its improved biological therapeutic functions. Although the molecular dynamics simulation showed inconclusive results regarding the stability of the protein-ligand complex, it revealed critical structural insights into the unstable binding mechanism. These findings provide a clear framework for optimizing and improving future BFP ligand designs. Altogether, this study provided valuable evidence and information on the medicinal chemistry of the BFP core, its synthetic derivatization, and perspectives on future design of potent and more selective BFP compounds utilizing various *in silico* methods.

ACKNOWLEDGMENT

The author would like to thank Assoc. Prof. Dr. Tanatorn Khotavivattana of Chulalongkorn University for the professional guidance. Special thanks to Prof. Dr. Paul Samuel Ignacio of the University of the Philippines Baguio for the assistance with the molecular dynamics simulation.

CONFLICT OF INTEREST

The authors declare that there is no conflict of interest.

CONTRIBUTIONS OF INDIVIDUAL AUTHORS

The author (R.E.) was responsible for conceptualization, experimental execution, and data analysis, as well as writing the original draft, reviewing, and editing the final manuscript.

REFERENCES

Agu PC, Afiukwa CA, Orji OU, Ezeh EM, Ofoke IH, Ogbu CO, . . . Aja PM. Molecular docking as a tool for the discovery of molecular targets of nutraceuticals in diseases management. Sci Rep 2023; 13(1). doi:10.1038/s41598-023-40160-2

Asghar U, Witkiewicz AK, Turner NC, Knudsen ES. The history and future of targeting cyclin-dependent kinases in cancer therapy. Nat Rev Drug Discov 2015; 14(2):130-146. doi:10.1038/nrd4504

Baell JB, Holloway GA. New substructure filters for removal of pan assay interference compounds (PAINS) from screening libraries and for their exclusion in bioassays. J Med Chem 2010; 53(7):2719-2740. doi:10.1021/jm901137j

Baell JB, Nissink JWM. Seven year itch: Pan-assay interference compounds (PAINS) in 2017—Utility and limitations. ACS Chem Biol 2018; 13(1):36-44. doi:10.1021/acschembio.7b00903

Berendsen HJC, van der Spoel D, van Drunen R. GROMACS: A message-passing parallel molecular dynamics implementation. Comp. Phys. Comm. 1995; 91:43–56.

Brachwitz K, Hilgeroth A. Synthesis and first biological evaluation of 1-aza-9-oxafluorenes as novel lead structures for the development of small-sized cytostatics. Bioorg Med Chem Lett 2002; 12(3):411-413. doi:10.1016/S0960-894X(01)00769-7

Brachwitz K, Voigt B, Meijer L, Lozach O, Schächtele C, Molnár J, Hilgeroth A. Evaluation of the first cytostatically active 1-Aza-9-oxafluorenes as novel selective CDK1 inhibitors with p-glycoprotein modulating properties. J Med Chem 2003; 46(5):876-879. doi:10.1021/jm021090g

Casimiro MC, Crosariol M, Loro E, Li Z, Pestell RG. Cyclins and cell cycle control in cancer and disease. Genes & Cancer 2013; 3(11-12):649-657. doi:10.1177/1947601913479022

Daina A, Michielin O, Zoete V. SwissADME: a free web tool to evaluate pharmacokinetics, drug-likeness and medicinal chemistry friendliness of small molecules. Sci Rep 2017; 7(1). doi:10.1038/srep42717

Daina A, Zoete V. A BOILED-egg to predict gastrointestinal absorption and brain penetration of small molecules. ChemMedChem 2016; 11(11):1117-1121. doi:https://doi.org/10.1002/cmdc.201600182

Dhavan R, Tsai LH. A decade of CDK5. Nat Rev Mol Cell Biol 2001; 2(10):749-759. doi:10.1038/35096019

Dong K, Wang X, Yang X, Zhu X. Binding mechanism of CDK5 with roscovitine derivatives based on molecular dynamics simulations and MM/PBSA methods. J Mol Graph Model 2016; 68: 57–67. doi:10.1016/j.jmgm.2016.06.007.

Doogue MP, Polasek TM. The ABCD of clinical pharmacokinetics. Ther Adv Drug Saf 2013; 4(1):5-7. doi:10.1177/2042098612469335

Eberhardt J, Santos-Martins D, Tillack AF, Forli S. AutoDock Vina 1.2.0: New docking methods, expanded force field, and python bindings. J Chem Inf Model 2021; 61(8):3891-3898. doi:10.1021/acs.jcim.1c00203

Ereje R, Yahuafai J, Jaroenchuensiri T, Supakijjanusorn P, Unson S, Toopradab B, . . . Khotavivattana T. Diversity oriented strategy (DOS) for the efficient synthesis of benzofuro[2,3-b]pyridine derivatives with anticancer activity. ChemMedChem 2025; 20(3):e202400514. doi:https://doi.org/10.1002/cmdc.202400514

Ertl P, Schuffenhauer A. Estimation of synthetic accessibility score of drug-like molecules based on molecular complexity and fragment contributions. J Cheminform 2009; 1(1):8. doi:10.1186/1758-2946-1-8

Goodsell DS, Olson AJ. Automated docking of substrates to proteins by simulated annealing. Proteins: Struct Funct Bioinf 1990; 8(3):195-202. doi:https://doi.org/10.1002/prot.340080302

Hay M, Thomas DW, Craighead JL, Economides C, Rosenthal J. Clinical development success rates for investigational drugs. Nat Biotechnol 2014; 32(1):40-51. doi:10.1038/nbt.2786

Holzer M, Schade N, Opitz A, Hilbrich I, Stieler J, Vogel T, . . . Hilgeroth A. Novel protein kinase inhibitors related to tau pathology modulate tau protein-self interaction using a luciferase complementation assay. Molecules 2018; 23(9):2335-2335. doi:10.3390/molecules23092335

Kramer B, Rarey M, Lengauer T. An alternative method for the evaluation of docking performance: RSR vs RMSD. J Chem Inf Model 2008; 48(7): 1411–1422. doi:10.1021/ci800084x.

Kusakawa GI, Saito T, Onuki R, Ishiguro K, Kishimoto T, Hisanaga SI . Calpain-dependent proteolytic cleavage of the p35 cyclin-dependent kinase 5 activator to p25. J Biol Chem 2000; 275(22):17166-17172. doi:10.1074/jbc.M907757199

Lenjisa JL, Tadesse S, Khair NZ, Kumarasiri M, Yu M, Albrecht H, . . .Wang S. Cdk5 in oncology: recent advances and future prospects. Future Med Chem 2017; 9(16):1939-1962. doi:10.4155/fmc-2017-0097

Lin JH, Yamazaki M. Role of p-glycoprotein in pharmacokinetics. Clin Pharmacokinet 2003; 42(1):59-98. doi:10.2165/00003088-200342010-00003

Lipinski CA. Lead- and drug-like compounds: the rule-of-five revolution. Drug Discov Today Technol 2004; 1(4):337-341. doi:10.1016/j.ddtec.2004.11.007

Liu JL, Gu RX, Zhou XS, Zhou FZ, Wu G. Cyclin-dependent kinase 5 regulates the proliferation, motility and invasiveness of lung cancer cells through its effects on cytoskeletal remodeling. Mol Med Rep 2015; 12(3):3979-3985. doi:10.3892/mmr.2015.3868

Meder L, Konig K, Ozretic L, Schultheis AM, Ueckeroth F, Ade CP, . . . Buettner R. NOTCH, ASCL1, p53 and RB alterations define an alternative pathway driving neuroendocrine and small cell lung carcinomas. Int J Cancer 2016; 138(4):927-938. doi:10.1002/ijc.29835

Meng XY, Zhang HX, Mezei M, Cui M. Molecular docking: A powerful approach for structure-based drug discovery. Curr Comput Aided Drug Des 2011; 7(2): 146-157. doi:10.2174/157340911795677602

Peyressatre M, Prével C, Pellerano M, Morris M. Targeting cyclin-dependent kinases in human cancers: From small molecules to peptide inhibitors. Cancers 2015; 7(1): 179-237. doi:10.3390/cancers7010179

Prasanna S, Doerksen R. Topological polar surface area: A useful descriptor in 2D-QSAR. Curr Med Chem 2009; 16(1):1-41. doi:10.2174/092986709787002817

Surabhi S, Singh BK. Computer aided drug design: An overview. J Drug Deliv Ther 2018; 8(5):504-509. doi:10.22270/jddt.v8i5.1894

Tell V, Mahmoud KA, Wichapong K, Schächtele C, Totzke F, Sippl W, Hilgeroth A. Novel aspects in structure–activity relationships of profiled 1-aza-9-oxafluorenes as inhibitors of alzheimer's disease-relevant kinases cdk1, cdk5 and gsk3β. MedChemComm 2012; 3(11):1413-1413. doi:10.1039/c2md20201h

Tian S, Wang J, Li Y, Li D, Xu L, Hou T. The application of in silico drug-likeness predictions in pharmaceutical research. Adv Drug Deliv Rev 2015; 86: 2-10. doi:10.1016/j.addr.2015.01.009

Topliss, J. G. Utilization of operational schemes for analog synthesis in drug design. J Med Chem 1972; 15(10):1006–1011.

Wei K, Ye Z, Li Z, Dang Y, Chen X, Huang N, . . .Chen G. An immunohistochemical study of cyclin-dependent kinase 5 (CDK5) expression in non-small cell lung cancer (NSCLC) and small cell lung cancer (SCLC): a possible prognostic biomarker. World J Surg Oncol 2016; 14(1). doi:10.1186/s12957-016-0787-7

Xie W, Liu C, Wu D, Li Z, Li C, Zhang Y. Phosphorylation of kinase insert domain receptor by cyclin-dependent kinase 5 at serine 229 is associated with invasive behavior and poor prognosis in prolactin pituitary adenomas. Oncotarget 2016; 7(32):50883-50894. doi:10.18632/oncotarget.10550

SUPPLEMENTAL INFORMATION

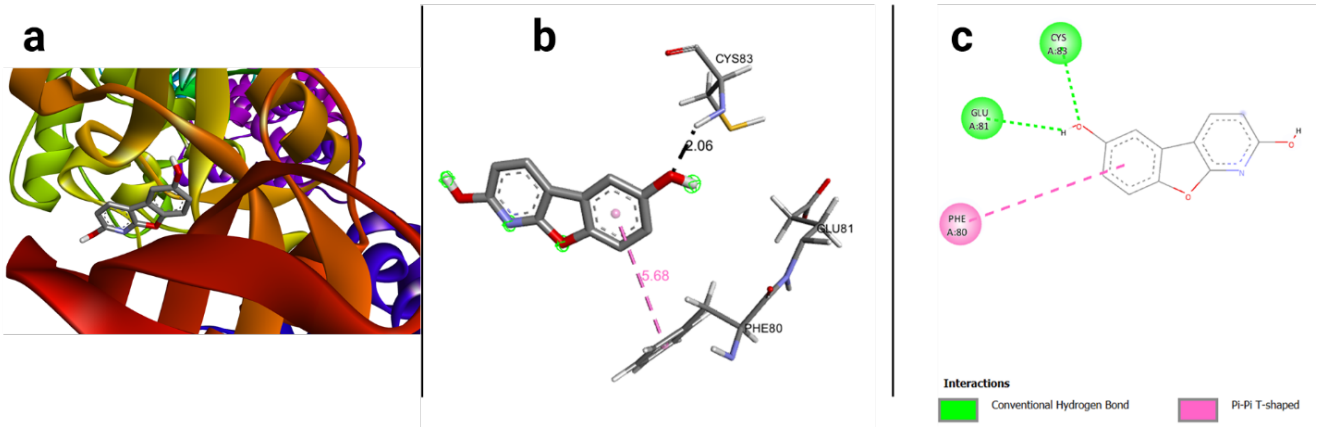

Figure S1: Preliminary molecular docking simulation of 2,6-dihydroxybenzofuropyrindine (2,6-dhBFP) with the CDK-5 enzyme. (**a**) Three-dimensional (3D) visualization of the binding pocket, (**b**) 3D simulation showing the interacting amino acids with the length of interactions in Angstrom, and (**c**) 2D visualization of ligand-enzyme complex with the type of interactions.

Table S1: List of derivatives in the **B**X-1-1 series and their corresponding binding affinities.

BX-1-1 Series					
Code	Binding affinity (kcal/mol)	Code	Binding affinity (kcal/mol)	Code	Binding affinity (kcal/mol)
B1-1-1	-9.1	B16-1-1	-9.9	B31-1-1	-9.9
B2-1-1	-9.0	B17-1-1	-10.2	B32-1-1	-9.8
B3-1-1	-8.9	B18-1-1	-10.1	B33-1-1	-10.0
B4-1-1	-9.3	B19-1-1	-9.8	B34-1-1	-9.9
B5-1-1	-9.3	B20-1-1	-9.9	B35-1-1	-10.0
B6-1-1	-9.9	B21-1-1	-10.0	B36-1-1	-9.9
B7-1-1	-9.8	B22-1-1	-9.7	B37-1-1	-9.9
B8-1-1	-10.1	B23-1-1	-9.9	B38-1-1	-9.9
B9-1-1	-10.1	B24-1-1	-9.9	B39-1-1	-10.1
B10-1-1	-9.8	B25-1-1	-9.7	B40-1-1	-10
B11-1-1	-10.0	B26-1-1	-10.0	B41-1-1	-9.3
B12-1-1	-10.0	B27-1-1	-10.3	B42-1-1	-9.3
B13-1-1	-9.9	B28-1-1	-10.5	B43-1-1	-9.6
B14-1-1	-10.0	B29-1-1	-10.7	B44-1-1	-9.8
B15-1-1	-10.1	B30-1-1	-10.3	B45-1-1	-9.4

Table S2: List of derivatives in the **B**1-**X**-1 series and their corresponding binding affinities.

B1-X-1 Series					
Code	Binding affinity (kcal/mol)	Code	Binding affinity (kcal/mol)	Code	Binding affinity (kcal/mol)
B1-1-1	-9.1	B1-12-1	-9.4	B1-23-1	-9.0
B1-2-1	-7.6	B1-13-1	-9.0	B1-24-1	-8.6
B1-3-1	-9.3	B1-14-1	-9.2	B1-25-1	-9.4
B1-4-1	-9.1	B1-15-1	-9.0	B1-26-1	-8.6
B1-5-1	-9.7	B1-16-1	-9.6	B1-27-1	-8.0
B1-6-1	-9.3	B1-17-1	-10.2	B1-28-1	-8.7
B1-7-1	-9.2	B1-18-1	-10.0	B1-29-1	-9.1
B1-8-1	-8.8	B1-19-1	-9.5	B1-30-1	-8.8
B1-9-1	-7.6	B1-20-1	-8.6	B1-31-1	-9.0
B1-10-1	-9.2	B1-21-1	-7.9	B1-32-1	-8.8
B1-11-1	-9.5	B1-22-1	-9.0	B1-33-1	-8.3

Table S3: List of derivatives in the **B**1-1-**X** series and their corresponding binding affinities.

B1-1-X Series					
Code	Binding affinity (kcal/mol)	Code	Binding affinity (kcal/mol)	Code	Binding affinity (kcal/mol)
B1-1-1	-9.1	B1-1-10	-9.5	B1-1-19	-9.7
B1-1-2	-8.6	B1-1-11	-9.4	B1-1-20	-9.7
B1-1-3	-8.4	B1-1-12	-9.4	B1-1-21	-9.5
B1-1-4	-9.0	B1-1-13	-9.5	B1-1-22	-9.5
B1-1-5	-8.7	B1-1-14	-9.1	B1-1-23	-9.4
B1-1-6	-8.7	B1-1-15	-9.7	B1-1-24	-9.3
B1-1-7	-8.9	B1-1-16	-9.8	B1-1-25	-9.3
B1-1-8	-8.9	B1-1-17	-10.1	B1-1-26	-9.7
B1-1-9	-9.8	B1-1-18	-10.2		

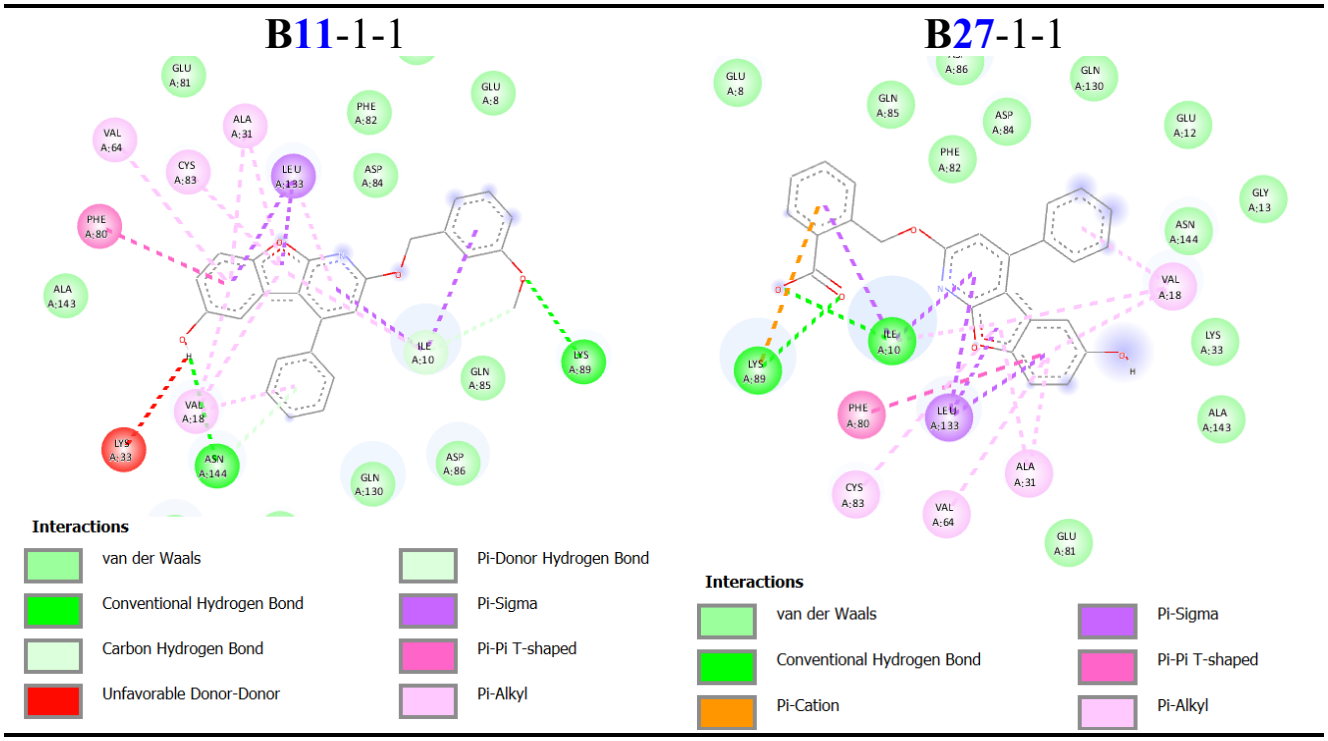

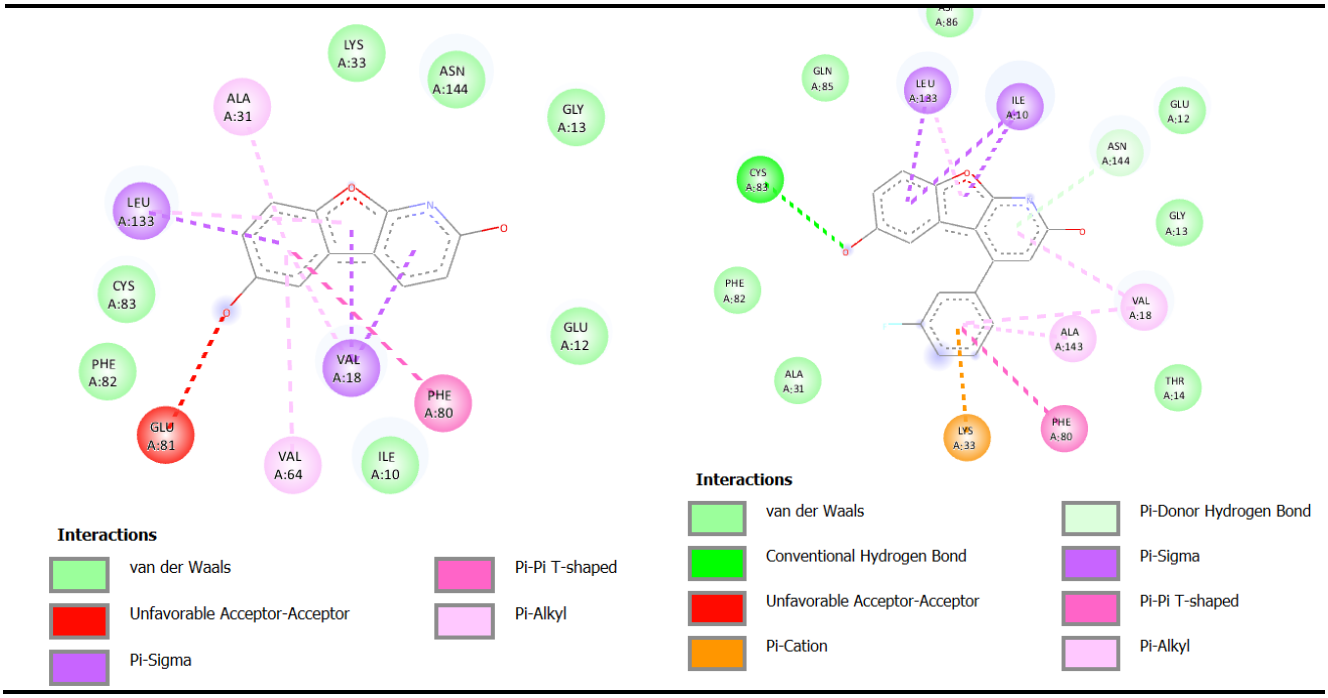

B1-17-1 **B1-1-9**

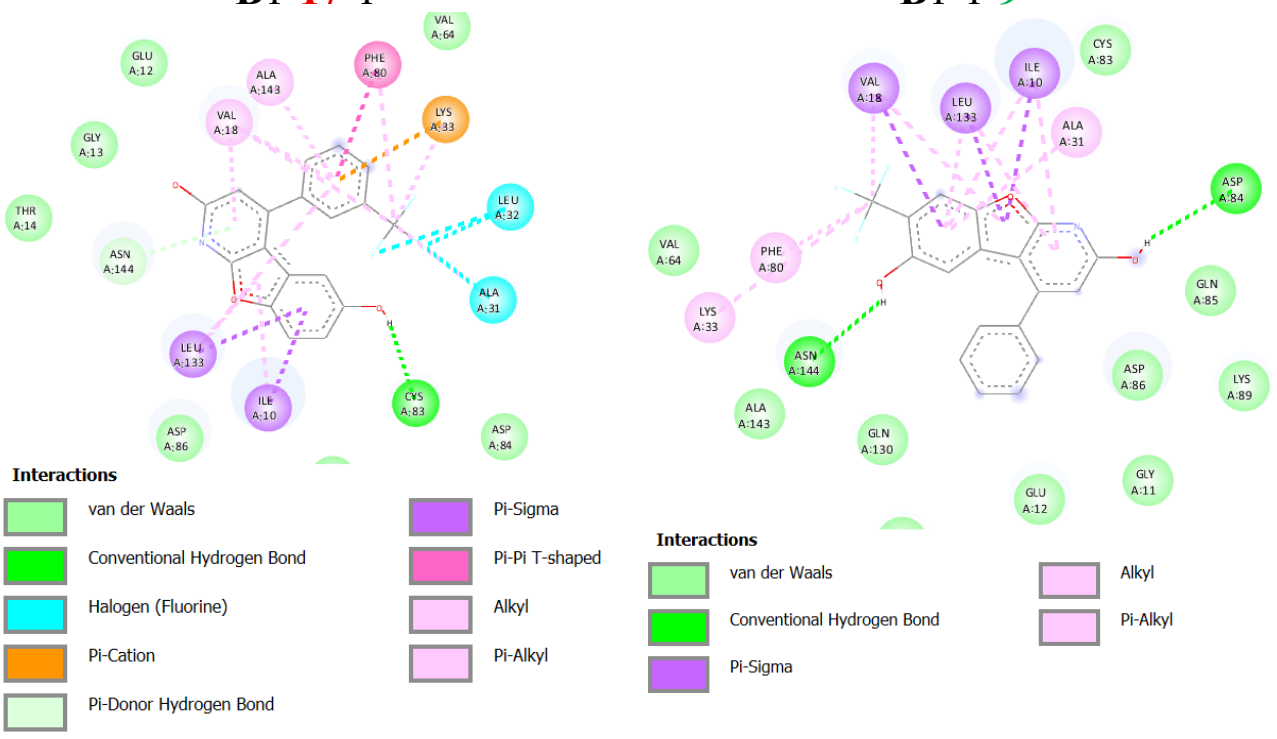

B1-1-17 **B1-1-18**

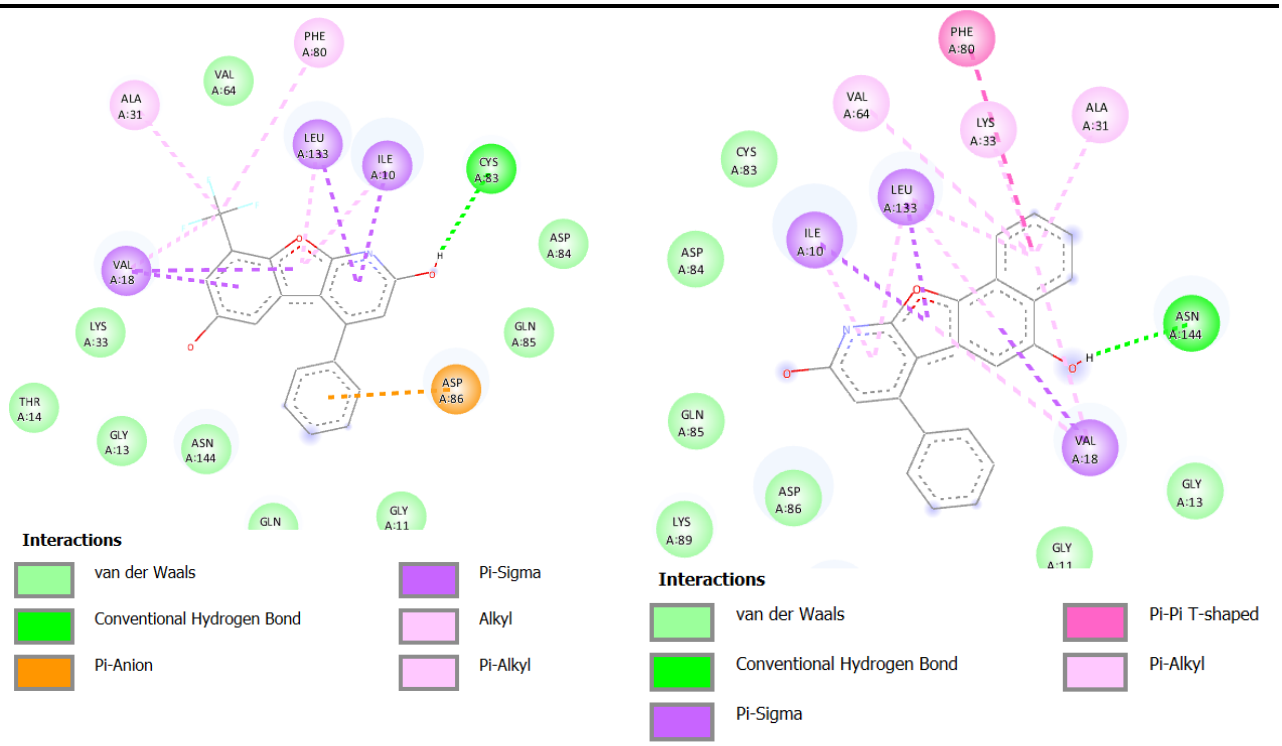

Figure S2: Two-dimensional (2D) interactions of the representative BFP ligands from the three derivatization series: **B**X-1-1, **B**1-X-1 and **B**1-1-X with the CDK-5 enzyme.